UNIVERSITY OF CALIFORNIA

SANTA CRUZ

A NOVEL WIRELESS SENSOR FOR AC CURRENT MEASUREMENT POWERED BY ENERGY HARVESTING

A thesis submitted in partial satisfaction of the requirements for the degree of

MASTER OF SCIENCE

in

COMPUTER ENGINEERING

by

Patrick Ayers

December 2018

The Thesis of Patrick Ayers is approved:

Professor Patrick Mantey, Chair

Professor Matthew Guthaus

Ali Adabi

Lori Kletzer
Vice Provost and Dean of Graduate Studies

Table of Contents

List of Figures

List of Tables

Abstract

A Novel Wireless Sensor
for AC Current Measurement
Powered By Energy Harvesting

by

Patrick Ayers

A prototype was designed, built, and tested that uses split-core current transformers to harvest electrical energy. These transformers can be easily attached around the AC lines of nearby machinery without interference to the electrical supply nor requiring the work of an electrician. This system requires virtually no maintenance as the endpoint energy harvesting devices require no batteries and can transmit messages periodically using energy harvested and stored in a capacitor bank. This system is able to take periodic measurements from a low energy Bluetooth transceiver, installed on a harvestable AC line carrying a minimum of $420mA$ (RMS) of current. Measurements increase in frequency as the harvested load power increases, and with the use of a prototype current transformer with a laminated steel core continuous operation with a $1.8v$ output can be acheived from as little as $6.25A$. This continuous operation allows for sampling rates as high as $12kHz$. The system itself draws no more than $250\mu W$ from the AC line it harvests from. These characteristics make the proposed system highly suitable for power measurement in important practical applications.

Dedicated to my parents. Thank you so much for always encouraging me to keep trying.

Acknowledgments

I would like to acknowledge Patrick Mantey, Stephen Petersen, Matthew Guthaus, Ali Adabi, Keith Corzine, Gabriel Elkaim, and CITRIS and the Banatao Institute for support and assistance.

Chapter 1

Introduction

The residential sector consumes roughly 22% of all energy in the United States,[8] yet obtaining detailed information on real-time personal power consumption is not readily available to the consumer. Often where energy sensors are to be deployed, conventional AC outlets are not available. There exist solutions for metering in these areas, however installation is complicated and involves some electrical wiring. This can be dangerous for consumers or require a professional, raising costs further. Metering devices are often installed in areas that are not frequently or easily accessed, making replacements of batteries impractical and costly for devices that are not powered by a connection to the supply mains. There exists a design trade-off with metering devices between ease of installation, cost, and maintenance needs. The solution developed in this thesis was to create a system that can collect energy from nearby AC conductors without direct contact, and convert that energy to charge a regulated DC power supply for a metering device. Recently there have been devices that use piezoelectromagnetic[16] and inductive[2] techniques to capture energy and remain easy to install. However, these devices were not designed to harvest energy to keep running continuously, instead they rely either on an external power source or intermittent operation.

The goal of this project was to investigate the potential of energy harvesting from an AC conductor and to design a system that can run continuously, harvesting energy from a $120v$ (RMS) AC line at the lowest current possible, in order to provide the greatest throughput of information. Also, by implementing a mesh network of wireless sensors, the task of metering may be subdivided and aggregated at a central hub, leading to a potential increase in accuracy.

To evaluate the proposed system, a prototype of the energy harvesting system was built after considering each component and its effects on overall efficiency. The harvesting system was benchmarked using test loads to simulate common household power consumption. It was found that the system can operate taking single periodic measurements with as little as $420mA$ of current on a $120v$ AC line simulating the transceiver sending data on the radio with greatest power output. The frequency of the periodic measurements increased with increasing AC loads. Further, it was shown that with a carefully designed harvesting system, continuous operation of the meter with up to a $12kHz$ sampling rate is possible with as little as $6.25A$ present on a breaker panel $120v$ AC conductor. Future improvements based on principles discussed in this thesis have the potential to lower the power needed from the AC line as efficiency is increased further.

Chapter 2

Related Work

Energy harvesting is currently implemented in many forms to power low energy sensor networks. In this section, recently designed harvesting systems are discussed. The methods of obtaining energy as well as the methods of data transmission are compared to the design discussed in this text to outline performance improvements and limitations.

2.1 Piezoelectric Harvesters

Piezoelectric elements with a set of permanent magnets at one end can be used to harvest energy from power lines containing AC current. This is done by converting the electromagnetic field into mechanical energy by means of vibrating the piezoelectric element arranged as a cantilever (see Figure 2.1) and then converting that vibration back into electrical energy [16]. One major advantage to this form of energy harvesting is that the piezoelectric element does not require any wrapping around the AC line and needs only to be placed in close proximity to the current carrying conductor. They can be tuned for resonance at $60Hz$ for the best energy conversion by choosing the appropriate materials and size for the

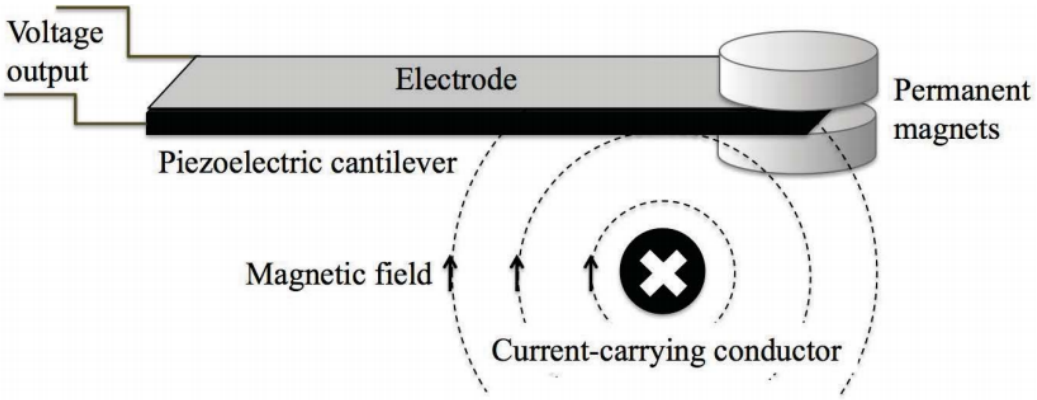

Figure 2.1: Model of a Piezoelectromagnetic (PEM) Energy Harvesting Device

constructed device. When attempting to use the piezoelectric element to both collect energy and measure AC current, there is an issue with crosstalk. Fields from adjacent power lines can influence the accuracy of a measurement as they will also affect the vibration of the piezo element. This makes a network of sensors in close proximity a great challenge to implement and obtain accurate measurement.

2.2 Monjolo Meter

This energy metering architecture developed at University of Michigan utilizes a single current transformer to power the system while also being used for measurement [2]. This method of energy harvesting can charge a capacitor to intermittently provide stable regulated voltage to a wireless sensor node. The manner in which power is measured with Monjolo is unique in that it counts the time between activations of the sensor node to estimate power consumption. It is assumed that the sensor node consumes a fixed amount of energy. Given this and the amount of energy that can be stored in the capacitor, the time between activations is roughly linearly correlated with the current draw of the primary AC

side of the current transformer. This simplification of the power measurement allows the sensor and microprocessor to draw minimal amounts of current. Due to measurements being derived from the time difference between packet transmissions, losses of packets will reduce the resolution of the measurement and therby its accuracy. The meter must account for lost packets by estimating average power assuming the load remains constant during the interval in which packets are dropped. This measurement scheme also does not account for the AC line voltage, adding additional inaccuracies due to estimation.

Chapter 3

System Overview

This section discusses the overall design of the energy harvesting supply and low power sensor and radio interface. The individual features of the system are discussed in simplified terms to highlight what is expected of the performance in a general sense. Real-world design limitations and drawbacks are introduced to produce a functional system that can be experimented with.

3.1 Data Collection Method

Due to the relatively small amount of current provided by harvesting from the AC conductor, the sensors themselves must be designed to minimize energy consumption. With this system, the transmitting sensors may be powered and send data periodically while the hub device waits to receive the data and compile it for the user to observe. In this instance, a smartphone application is used to recieve the Bluetooth information from the energy harvesting sensor. With a split-core current transformer, the sensor measures voltage across a load resistor to give an analog reading of the current in the AC line.

A diagram of this proposed sensor network is shown in Figure 3.1.

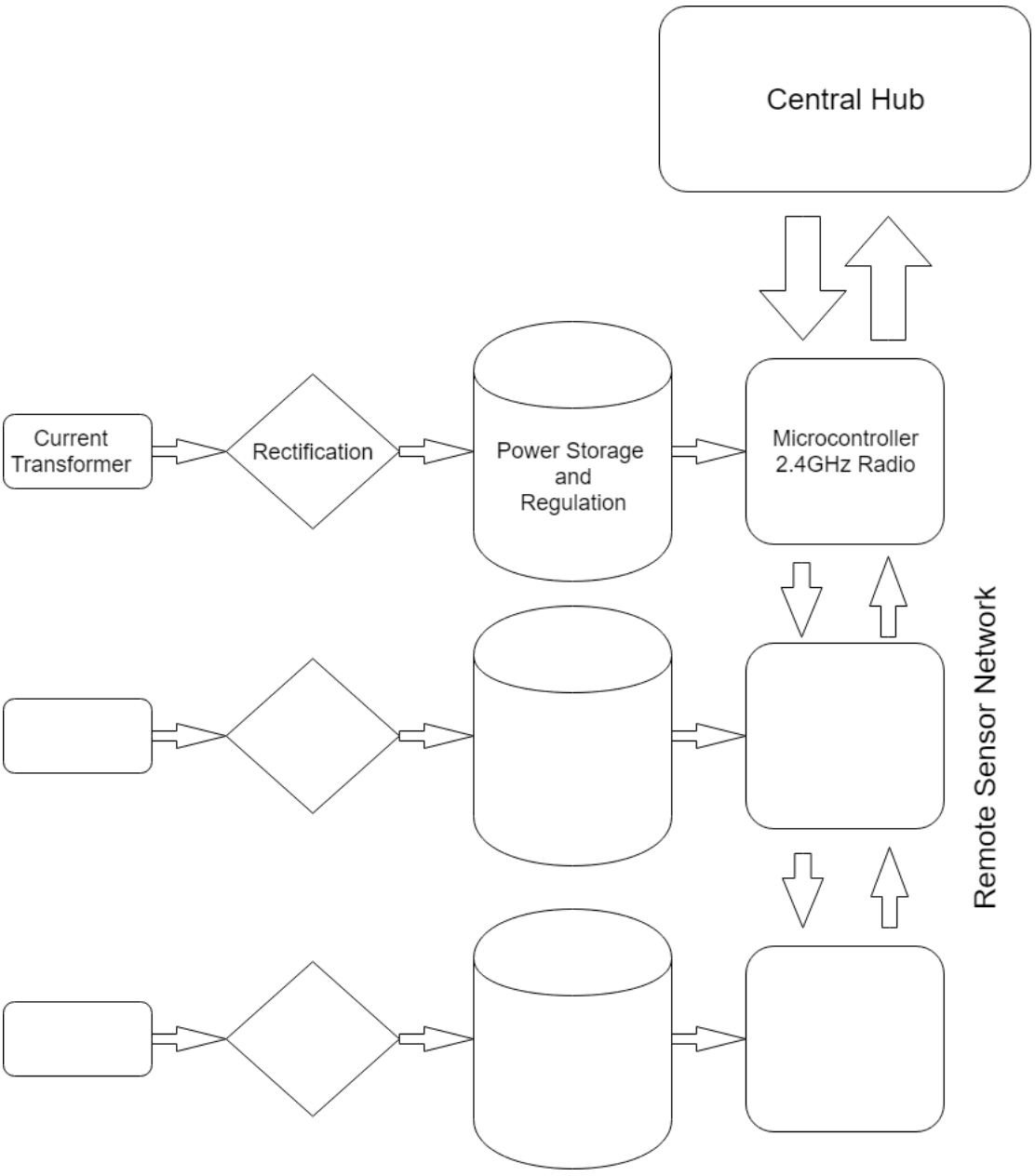

Figure 3.1: Overview of network of low power, energy harvesting remote sensors.

3.2 Energy Harvesting Scheme

An estimate of magnetic field strength can be made by treating the AC line as if it were an infinitely long conductor. The flux density B at a point distance r from the conductor is given by the formula $B = \frac{\mu I_o}{2\pi r}$[4] where μ is the permeability of the material, I_o is the peak amplitude of the current in the conductor, and ω is the frequency of the current. The controllable variables in an energy harvesting system are the permeability of the chosen material μ and the distance from the conductor r. From this equation, it can be seen to achieve the highest possible flux density B and thereby harvest the most energy, the harvester must be placed as close as possible to the conductor (small r), and a high permeability material should be used (large μ). The design chosen for the experiments conducted in this thesis utilized a split-core current transformer attached around an AC conductor to convert the present magnetic field into an AC voltage. This technique was chosen because a transformer containing a core material has greater permeability than alternatives such as Rogowski coils which lack a rigid core. Completely encircling the conductor in a core of high permeability ensures the best magnetic coupling. The use of a split core provides less current than a solid core due the the reluctance caused by the air gap in the core; however, this drawback is outweighed by the ease of installation that a split core design provides. No disruption of the power lines is necessary when the transformer is attached to the wire. Making sure that the two halves of the split core are fastened tightly together ensures that a minimal amount of flux leakage occurs. A diagram of the construction of a split-core current transformer along with that of a Rogowski coil are displayed in Figure 3.2.

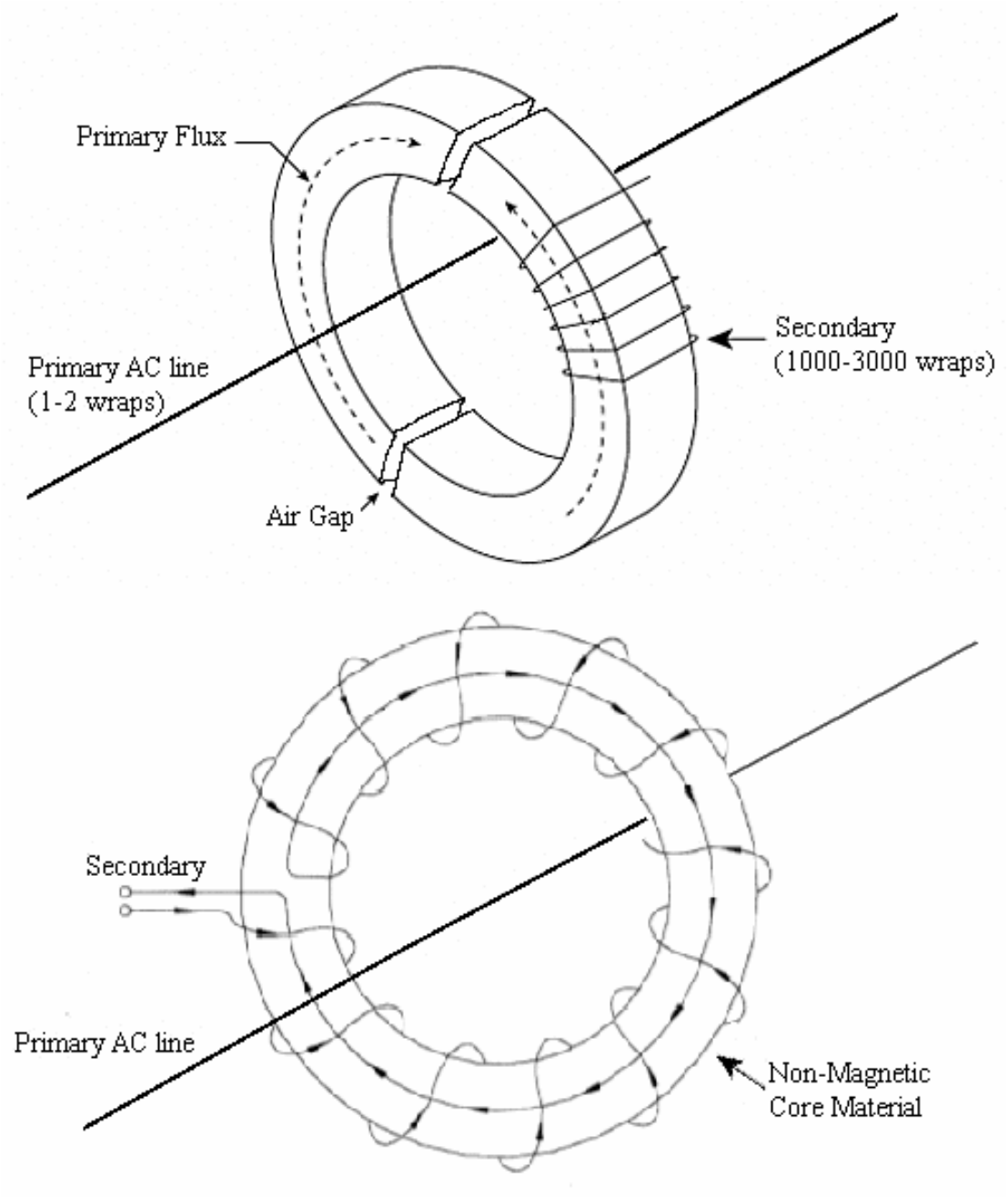

Figure 3.2: Diagrams of basic construction and operation of a split-core current transformer (top) and Rogowski coil (bottom).

Chapter 4

Design Implementation

To ensure that the general design concept for the energy harvesting sensors is viable, a prototype system was constructed for testing. This system was designed to be modular so that individual components of the system could be interchanged to test thier effects on performance. The details of the contruction of the system as well as the individual components tested are explained in this section.

4.1 Split-Core Transformer Construction

In order for the rectifier and voltage regulation circuitry (seen in Figures 4.2 and 4.3) to operate and power the microcontroller, a minimum operating voltage is required. The desired performance for the transformer is to meet this minimum voltage requirement on the output winding for the smallest primary AC load possible. This will allow the power meter to be capable of performing useful measurements across the widest range of loads. A higher ratio on the output will create a larger voltage, but in turn less usable current will be present to be harvested. It is also important to note that voltage in this design is limited to $20v$ by a Zener diode to protect the DC voltage converter to be discussed in section

4.2. Increasing the AC voltage on the output winding beyond the $20v$ limitation is inefficient. The transformer must also create enough magnetic coupling to the primary to keep the buck regulator operating for a duration long enough for a System on a Chip (SoC) to power up and send a sensor measurement over a radio transceiver. If multiple or continuous sensor measurements may be taken, the accuracy of the system improves. The placement of the primary winding around the core itself is important. Affixing it tightly around the bottom half of the U section of the core ensures flux leakage is minimized as there are less losses to the environment and also the the opening end of the split core. Inductance of the transformer can be approximated by the equation $L = \frac{N\Phi}{I} = N^2(\frac{1}{R_c+R_g})$[6] where N is the transformer ratio, I is current, Φ is flux, and R_c and R_g are core and gap reluctance. In a split-core current transformer, the reluctance of the air gap is quite large due to the gap being significant (larger than 10μm). In this case, R_c can be ignored and the equation $L = N^2\frac{\mu_o A_g}{g}$[6] models the transformer inductance with A_g being gap area and g being the gap distance. This equation explains how even a small increase in gap distance or decrease in core area has an impact on performance.

Next core materials and construction methods must be considered as they determine the maximum flux density inside the core as well as the amount of losses due to eddy currents and hysteresis. The variety of commerical split-core current transformers that were available to experiment with all contained ferrite cores. This material offers a high resistivity to keep eddy current losses low, but it also offers a quite low maximum flux density of around 0.3 to 0.5 Tesla. To experiment with a material with a higher saturation level, a custom current transformer was constructed using 2 U cores made of laminated silicon steel with a maximum flux density around 1.3-1.5 Tesla. The laminated layers separated

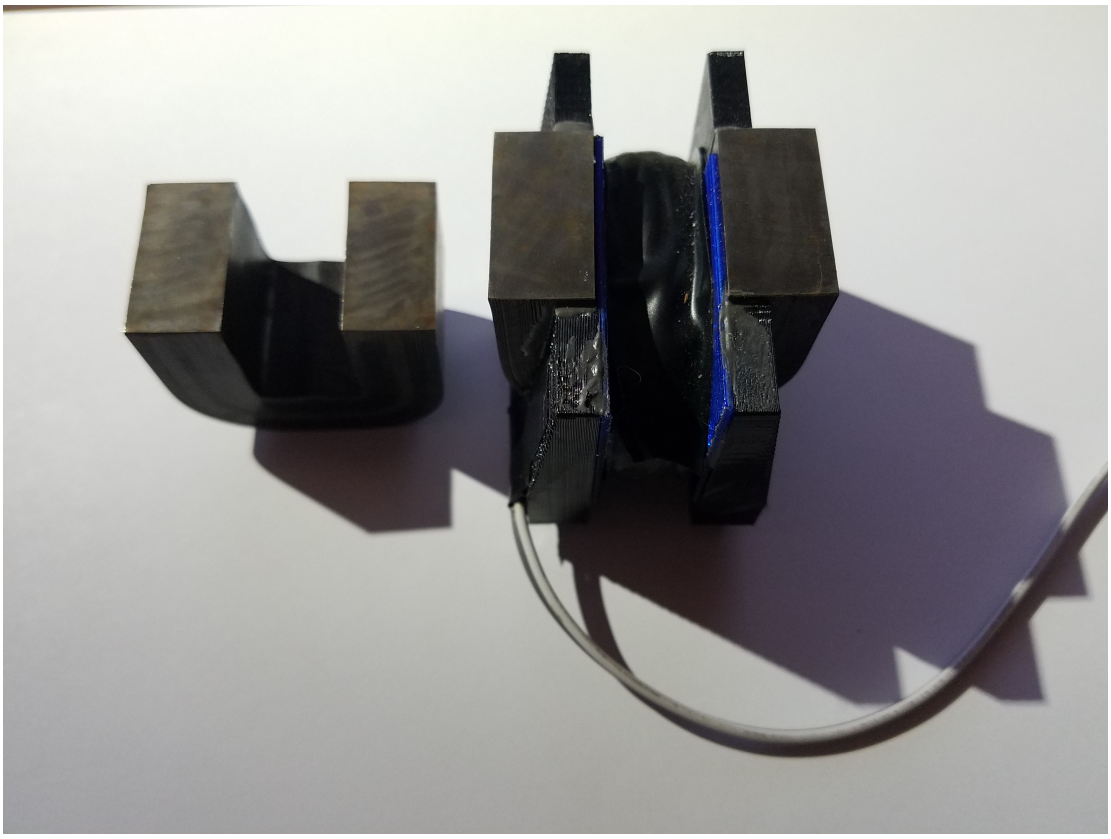

Figure 4.1: Laminated steel core current transformer wound with 30AWG coated wire and 3d printed housing.

by insulating adhesive also served to keep eddy current losses low. The custom prototype transformer can be seen in Figure 4.1. The cross sectional area of each core is also considered when taking measurements, as more area should allow for more flux at a given possible flux density. The major sources of energy loss to minimize in the transformer are the magnetizing inductance and series resistance in the secondary windings. A general equation for the winding inductance is given by $L_m = \frac{N_2^2 A_c \mu_c}{l_c}$[6] Where N is the secondary transformer ratio, A_c is the core cross section area, μ_u is the core permeability and l_c is the flux path length around the core. As can be seen, there is a diminishing return to increasing permeability and core area as magnetizing inductance losses also increase. Lowering the number of

secondary turns decreases both resistive and inductive losses, however there must be a high enough secondary ratio to produce useful voltage for the regulator. The resistance in the primary conductor is very low. With typical wire gauges of around 8-16 and a few amps of current as would be present when measuring loads in the 100-1000W range of the experiment, a voltage drop of around a few millivolts should be expected. The high ratio of the secondary winding of a current transformer allows for this small voltage to be raised to a voltage that can be rectified and used by the buck converter to generate a stable DC voltage. The greater the ratio however, the lower the amount of current that is present on the secondary as well. Because the buck converter has an operting input voltage threshold between $2.7v$ and $20v$, it is important to have a transformer ratio that meets an acceptable minimum operating voltage for a sufficiently small minimum AC load and to keep this ratio as low as possible to achieve the greatest possible secondary current. The easiest method of manipulating the turns ratio of the preconstructed current transformers is to increase the number of windings of the primary AC line through the core. This however, must be kept to a maximum of 2 or 3 turns as it would be difficult to install without altering the existing AC lines if more wraps were desired. Increased turns also serve to increase the voltage drop across the primary as there is more resistance to the current passing through the current transformer with the increased length of wire. However, this increase in resistance is fairly small in magnitude.

4.2 AC Energy Collection

In order to convert the AC current created in the transformer into a usable DC current for a microcontroller, the LTC3588 from Linear Technologies was used[7]. This IC is designed primarily to harvest energy from piezoelectric elements, and

because of this it features a low-dropout bridge rectifier and an efficient buck regulator to output a fixed voltage from a small current stored on an input capacitor. The LTC3588 has an operating rage of $2.7v$ to $20v$ and the input is shunt protected meaning it can provide useful output voltage over a wide range of loads where the AC voltage in the transformer will vary greatly. When there is not enough current present to continuously operate the buck converter, the IC enters an undervoltage lockout (UVLO) mode using less than a milliamp while the rectifier stores energy on the input capacitor. This enables periodic operation, even with small AC loads. The buck converter can efficiently provide up to $100mA$ of current, which exceeds the requirements for the transceivers considered. An example of the circuit used in this energy harvesting scheme can be seen in Figure 4.2. As can be seen, the critical points of adjustment in the circuit are the input capacitor on V_{IN}, the capacitor on the switching output, and the switching inductor. There are also four selectable output voltages that all lie within the range of operation of a low energy transceiver.

4.2.1 Capacitor Considerations

The input capacitor stores energy for each activation of the buck converter, therefore a greater capacitance allows for a longer runtime. The drawback to this is that the time it takes to charge the capacitor is increased and thus the frequency of operations decreases. It is important, regardless of the frequency of operation, that when the converter activates it provides a stable voltage long enough to take at least one sensor reading. The aim was to achieve at least $25ms$ of operation across all measurable AC loads to ensure one reading with most modern transceivers. In the majority of testing the output voltage was $3.3v$. At this voltage the storage reaches a threshold of about $5.25v$ and continues to supply

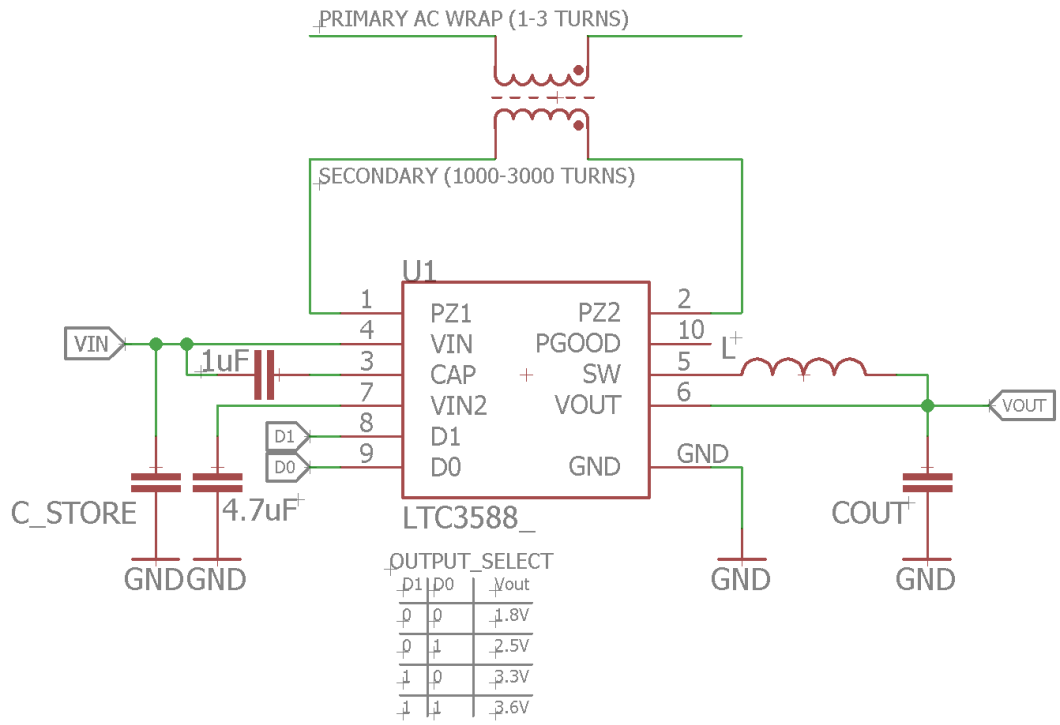

Figure 4.2: Schematic showing input and output capacitors and the switching inductor.

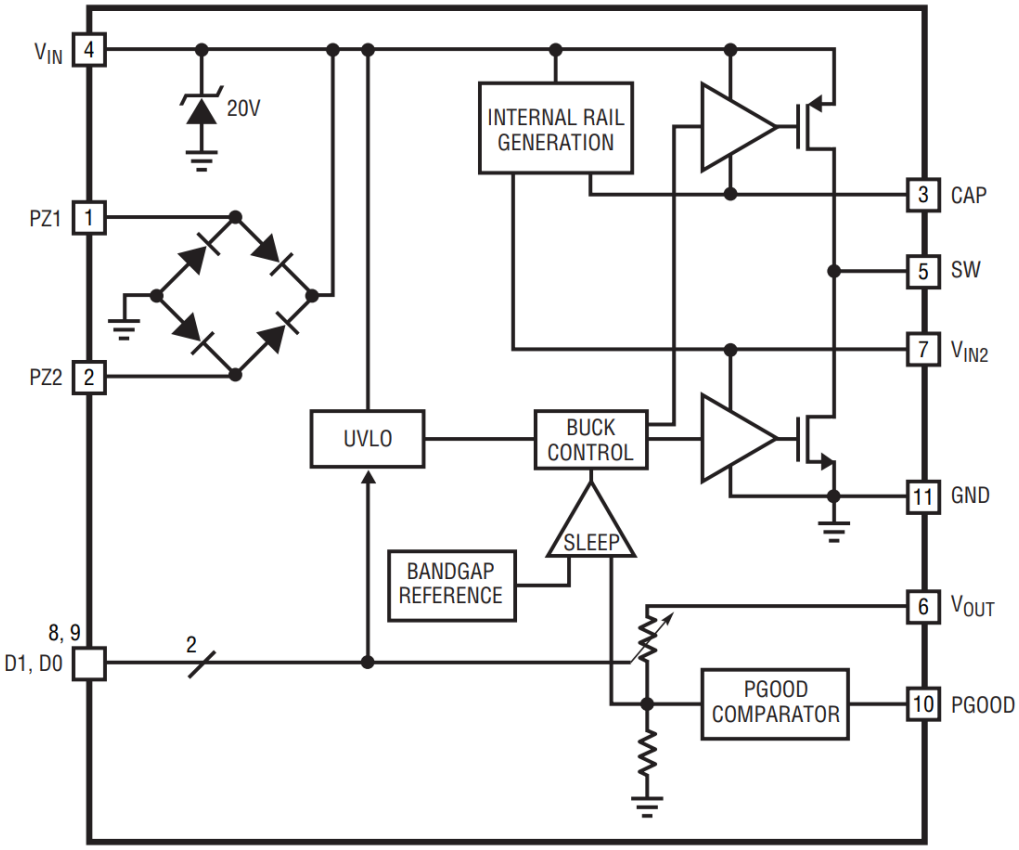

Figure 4.3: Block diagram of the internal circuitry of the LTC3588 [7].

Capacitor Type	DCL (nA)	ESR (mΩ)	Price
Aluminum Electrolytic	63	1218	$0.25-$1.25
Tantalum Polymer	52	792	$1.80-$3.20
Ceramic MLCC	11	724	$3.00-$5.25

Table 4.1: Table of tested capacitor types. Prices based on single quantity availability on Digikey for $220\mu F$ $16v$.

until around $3.8v$. The equation for capacitor discharge is $V_c = V_0 e^{-t/RC}$. Given a typical load of around 220Ω a capacitance of around $350\mu F$ should provide output for $25ms$. For this reason $220\mu F$ and $440\mu F$ were the tested input capacitance values. The type of capacitor used should have low levels of internal losses for the best performance. The amount of energy to be harvested is often small enough that internal losses can significantly affect charging time for the LTC3588 and also affect duration of stable output voltage. Aluminum electrolytic, tantalum polymer, and multilayer ceramic type capacitors were chosen to test a range of prices and compositions. DC leakage current (DCL) is measured at $3.5v$ which will be typical during a charging cycle. Series resistance (ESR) was measured on an LCR meter at a frequency of $100Hz$ which is fairly close to the $60Hz$ that will be experienced. All capacitors tested are $100\mu F$ $16v$ in value. The results of the capacitor comparisons can be seen in Table 4.1.

As can be seen, multilayer ceramic capacitors offer significantly lower DC leakage than other types of capacitor. However, ceramic capacitors of this rather large value and voltage rating are more expensive. They are also more fragile in construction than the other capacitor types making them more prone to failures. Tantalum was the chosen capacitor type for the majority of tests because they

are available in a compact size with the required capacitance value for a relatively low cost. Tantalum capacitors also have a lower DC leakage and ESR than electrolytic type capacitors and have long term reliability where electrolytics suffer from failing dielectric materials over time.

4.2.2 Switching Inductor Considerations

As mentioned by the LTC3588 datasheet, the internal buck converter is optimized to function with an inductor between $10\mu H$ and $22\mu H$. However with higher input voltages near the the $20v$ limit, efficiency can be increased with a larger inductance value. This increase in inductance in turn increases the on-time of the PMOS which supplies current into the inductor and reduces gate charge losses. In order to compare the performance impact of changing this inductance, $10\mu H$, $47\mu H$, and $220\mu H$ inductors were tested in circuit. All parts were of the same series made by the same manufacturer to ensure that each has similar specifications other than the inductance value itself.

4.3 Transceiver SoC Selection

To keep the design efficient and compact, the requirement is to use an SoC which combines a low-power microcontroller and a radio transceiver. Minimizing the voltage and current requirements for a transmission is a key part of the design while also maintaining a reasonable $20 - 50ft.$ range between the hub and the sensors. The frequency on which the SoC will transmit sensor readings is a crucial design parameter. Lower frequency transmitters that operate under $1GHz$ offer the best range for the current draw and allow for the best penetration through walls where the sensors are likely to be placed. The trade-off is that the

transmitter antenna itself must be larger in size to follow the quarter wavelength rule for optimal transmission distance. Also, current manufacturers of sub $1GHz$ transceivers typically employ proprietary protocols that limit interoperability between different hardware. Regional restrictions on sub $1GHz$ also tend to vary more. $2.4GHz$ protocols such as Zigbee and BLE are more widely supported and transceivers can be built with compact, PCB trace antennae. Mesh networking is supported by $2.4GHz$ protocols and thus with the use of strategically placed receiver hub devices, the range of the network can be extended greatly. The $2.4GHz$ band however is quite crowded with other technologies that can lead to collisions during transmission. In the case of the energy harvesting transmitter design, minimal current draw is key and limiting the number of radio activations to send one message greatly impacts the overall duty cycle of data transmissions. For ease of use in the home and with smartphones and other bluetooth devices, $2.4GHz$ was the chosen frequency of transmission for the current design. In the future, a sub $1Ghz$ can also be designed to better handle the larger interference found in industrial settings. The increased range would also benefit customers who wish to use the transmitters in remote environments such as farms and mining operations. For testing considerations, a range of popular microcontrollers with integrated BLE for low power sensor applications were compared. A breakdown of some key specifications of the different SoCs can be seen in Table 4.2. For experimentation, the nRF52832 was chosen as its radio and CPU both offer considerable performance for thier low current draw. The nRF52832 is also readily available in breakout development kits at a low cost and there is support and helpful documentation online to aid in prototyping.

Model Name	Operating Range[v]	Memory	CPU	CPU Efficiency	Radio Current(RX) @3v	Radio Current(TX) @3v	RX Sensitivity
ST BlueNRG-2	1.7v-3.6v	256k Flash, 24k RAM	ARM Cortex-M0 32MHz	1.9mA Typical	7.7mA @ 1Mbps	+8dBm 15.1mA +4dBm 10.9mA +2dBm 9mA -2dBm 8.3mA -8dBm 7.1mA	-92dBm
Nordic Semiconductor nRF51822	1.8v-3.6v	256k Flash, 32k RAM	ARM Cortex-M0 32MHz	1.4mA Typical	9.7mA @ 1Mbps	+4dBm 11.8mA 0dBm 8.0mA -4dBm 6.3mA	-90dBm @ 1Mbps -96dBm @ 250kbps
Nordic Semiconductor nRF52832	1.7v-3.6v	512k Flash, 64k RAM	ARM Cortex-M4 64MHz	3.8mA Typical (58uA/MHz)	5.4mA @ 1Mbps 5.8mA @ 2Mbps	+4dBm 7.5mA 0dBm 5.3mA -4dBm 4.2mA -8dBm 3.8mA	-93dBm
NXP QN908x	1.65v-3.6v	512k Flash,// 128k RAM	ARM Cortex-M4F 32MHz	1.4mA Typical	3.5mA @ 1Mbps 5.0mA @ 2Mbps	0dBm 3.5mA	-95dBm
Texas Instruments CC2650	1.8v-3.8v	128k Flash, 28k RAM	ARM Cortex-M3 48MHz	2.95mA Typical (61uA/MHz)	5.9mA @ 1Mbps	+5dBm 9.1mA 0dBm 6.1mA	-97dBm

Table 4.2: List of competing low power microcontrollers with BLE.

Chapter 5

Performance Evaluation

This section describes the experiments performed on the prototype energy sensor discussed in the previous section. These experiments help to evaluate theoretically how well the system functions as a home energy meter. The tested prototype can be seen in Figure 5.1.

5.1 Experimental Setup

In order to test the performance of the energy harvesting system, a test load was implemented using switchable incandescent bulbs and heating elements. While this experiment did not account for inductive or capacitive loads, many household devices consuming more than $100W$ are required to have power factor correction circuitry that makes them behave close to a purely resistive load[15]. The switchable loads provided a range of data for AC loads between $50 - 800W$. This range was chosen as the typical minimum load of a household is generally around this amount. By designing the harvesting system to provide an acceptable supply of power in this range, the system could operate with some data throughput nearly constantly without interruption. The NRF52832 was programmed with

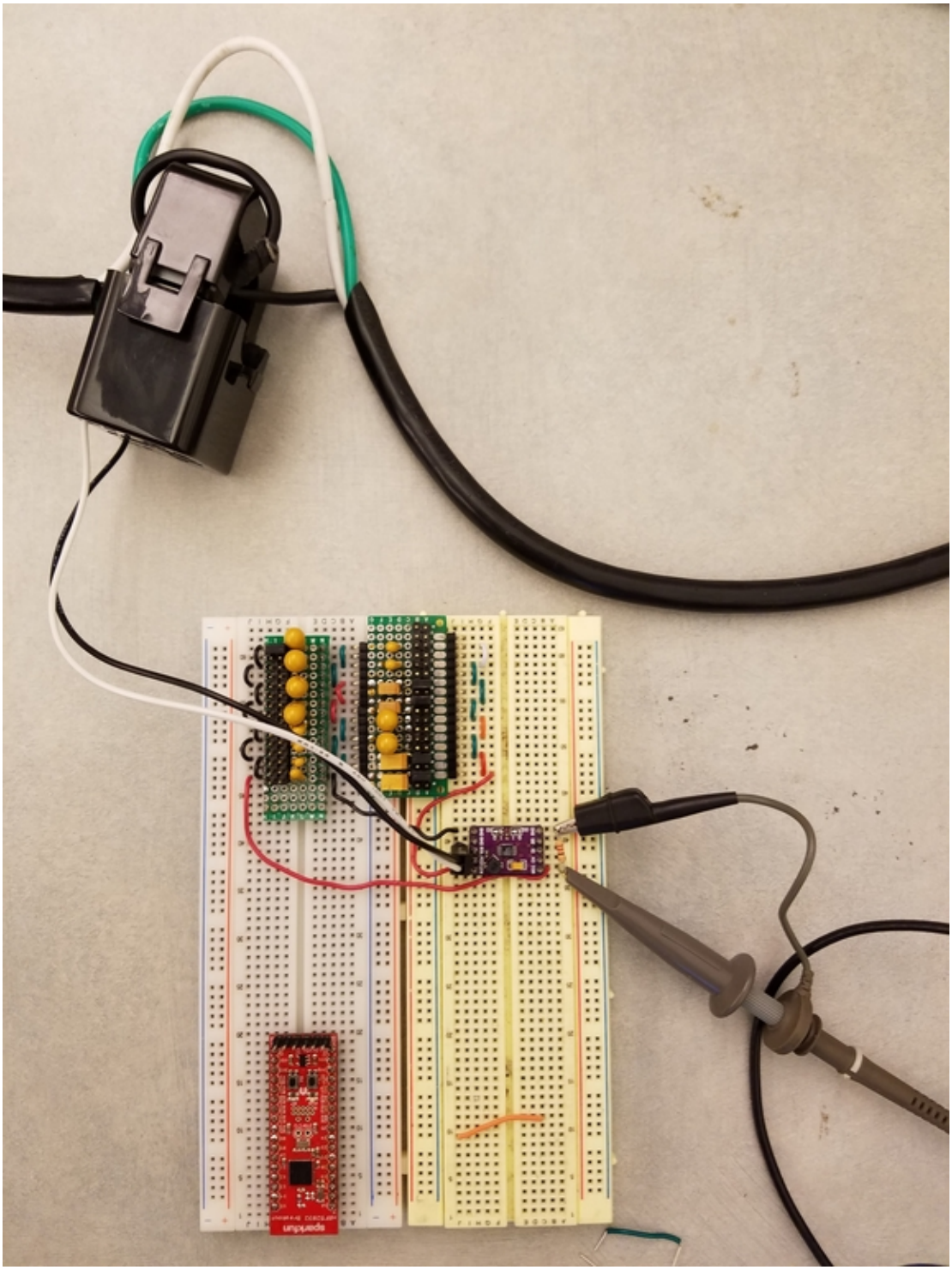

Figure 5.1: Test setup of the energy harvesting supply with dummy load resistor and adjustable input and output capacitor boards.

a simple routine reading a value from the ADC. This was measuring the voltage across a resistance placed in parallel with the secondary winding of the current transformer. This was sent using BLE over the transceiver on a loop. This rapid use of the transceiver was meant to find an estimate of the highest possible current consumption to expect from the system. In this configuration, the transceiver is capable of sending current readings with a sampling rate measured at about $12kHz$. The current draw from the SoC is found to be $10.91mA$ with the operating voltage at $3.3v$ in this scenario. In order to simulate this as a constant load, a resistor measured to be 216.2Ω was connected to the output of the LTC3588.

5.2 Test Parameters

To devise an energy harvesting system with the greatest performance in the tested range of AC loads, all the adjustable factors of the circuit were analyzed in detail beginning with the current transformer to be attached to the current-carrying AC line. In order for the transformer to transmit the most energy from the primary to the secondary winding, its saturation point must be maximized. This allowed for the highest possible flux density B in the core for a given magnetizing force H. This force in the core material is roughly equal to $I * N/length$. Therefore by increasing the diameter of the core and reducing the number of secondary turns, the magnetizing force is kept low and saturation is prevented. Figure 5.2 is a graphical representation of the realtion between flux density and magnetizing force and is known as a B-H curve. Visually it can be seen that in order to increase the flux density for a given magnetizing force, the coercive force must be minimized. This force opposes the flow of current on each AC cycle and is a hysteretic source of energy loss. It can also be seen that saturation can be raised by increasing the overall slope of the graph. This relationship of B/H or

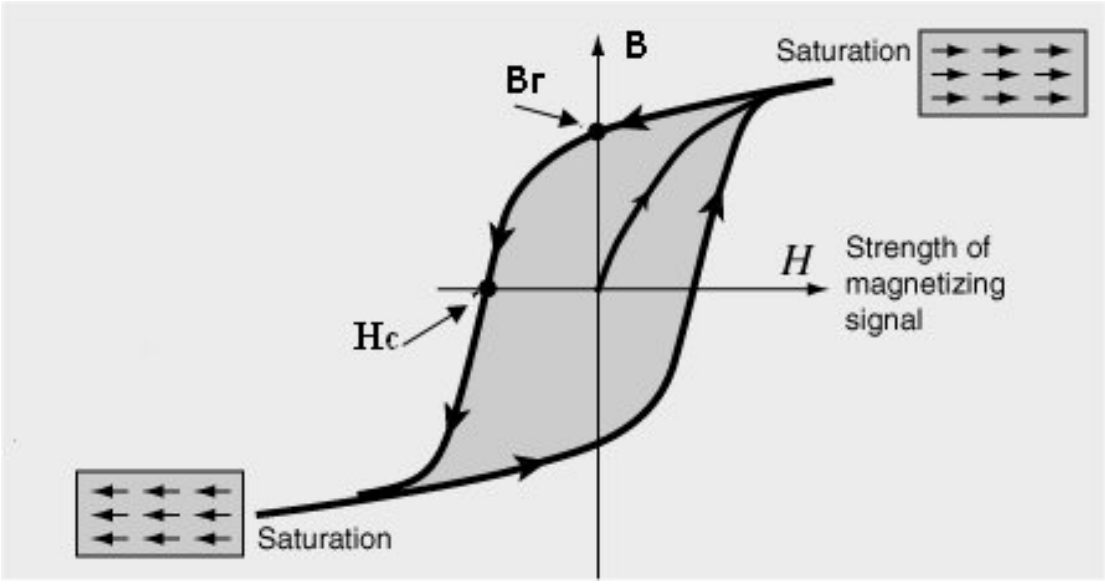

Figure 5.2: Curve relating flux density to magnetizing force in a core material. Note that B_r is residual magnetism and H_c is the coercive force.

flux density to magnetizing force is the permeability of the material, and its value greatly affects the performance of the transformer. This permeability is largely due to the electromagnetic properties of the material. To increase overall flux in the material, the cross sectional area can also be increased for a set flux density.

5.2.1 Results

In the tests conducted, four different current transformers were compared. The detailed specifications of each can be seen in Table 5.1.

For the first test, the system was tested with the primary passing through the transformer core a single time. The prototype transformer was used in conjuntion with $220\mu F$ of input capacitance and $10\mu F$ of output capacitance on the LTC3588. All capacitors used were tantalum. The LTC3588 was set to output $3.3v$ and was using a $10\mu H$ switching inductor. The primary was then wound around the core to create 2 loops, effectively halving the turns ratio. The results of this comparison

List of Tested CTs			
Model Name	Cross Section Size [mm]	Turns Ratio	Core Material
SCT-013 000	6x6.5 ($39mm^2$)	1:2000	Ferrite
OPCT10AL	5x11 ($55mm^2$)	1:3000	Ferrite
CTL-24-CLS	7x14.75 ($103.25mm^2$)	1:2000	Ferrite
Custom Design	13x25.5 ($331.5mm^2$)	1:1000	Laminated Steel

Table 5.1: Comparison of the current transformers tested.

can be seen in Figure 5.3. By wrapping another primary winding and lowering the output ratio, the output current was also raised while keeping the voltage within an range acceptable for the buck converter. For the purposes of the tested system, 2 wraps around the core provided much greater performance while still remaining relatively easy to install. All further measurements were taken using the CTs in this configuration with 2 wraps tightly bound the the core section. An example of this configuration is seen in Figure 5.1.

Next, all four current transformers were tested together to compare them on the basis of core area and composition. Each setup was identical in every way with the same $220\mu F$ input capacitance, $10\mu F$ output capacitance, and $3.3v$ output voltage set. The period of time between each activation of the boost converter and the time it remained active at the set output voltage were recorded using the experimental AC load setup. Figure 5.4 shows this data compiled together to represent the overall duty cycle of boost converter active time over AC load power.

As can be seen, the performance of all the commercial current transformers varied little with core size and secondary turns ratio. One of the major limitations of these transformers were their ferrite cores with relatively low permeability.

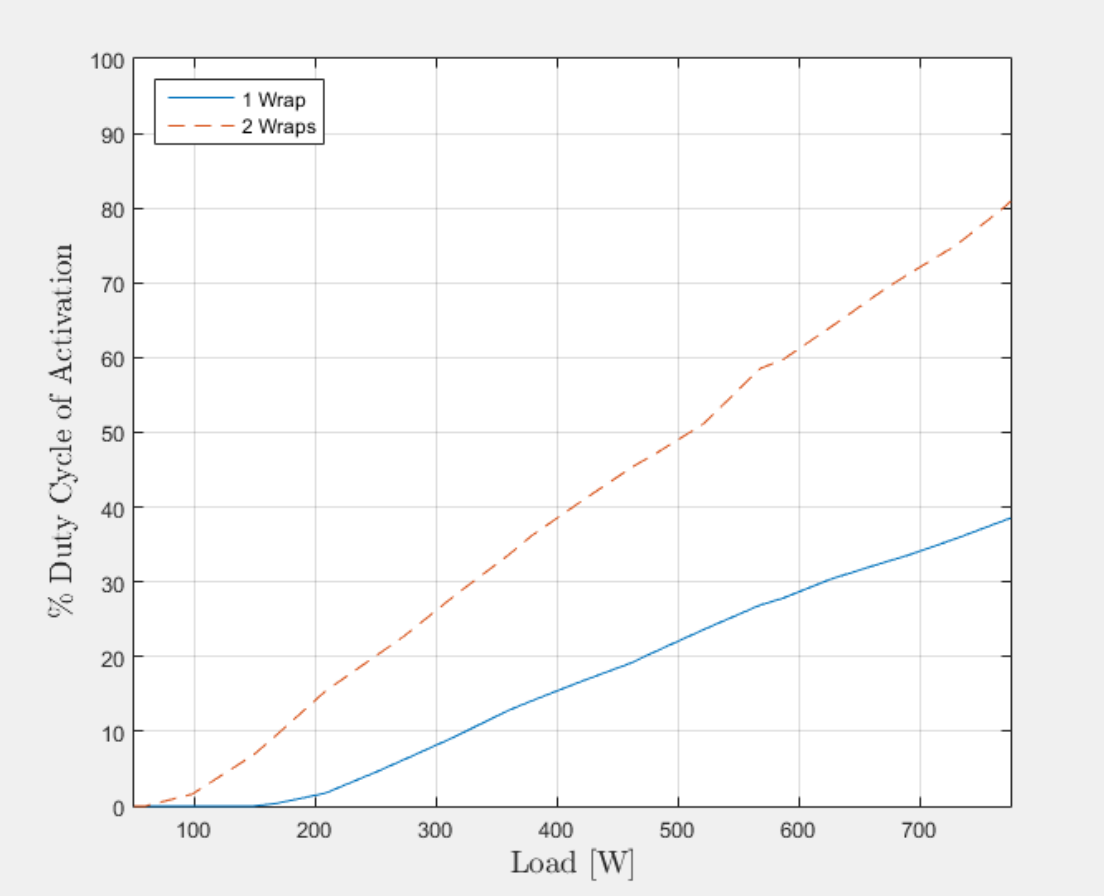

Figure 5.3: This graph demonstrates the performance difference obtained by varying the number of times the primary conductor passed through the transformer core.

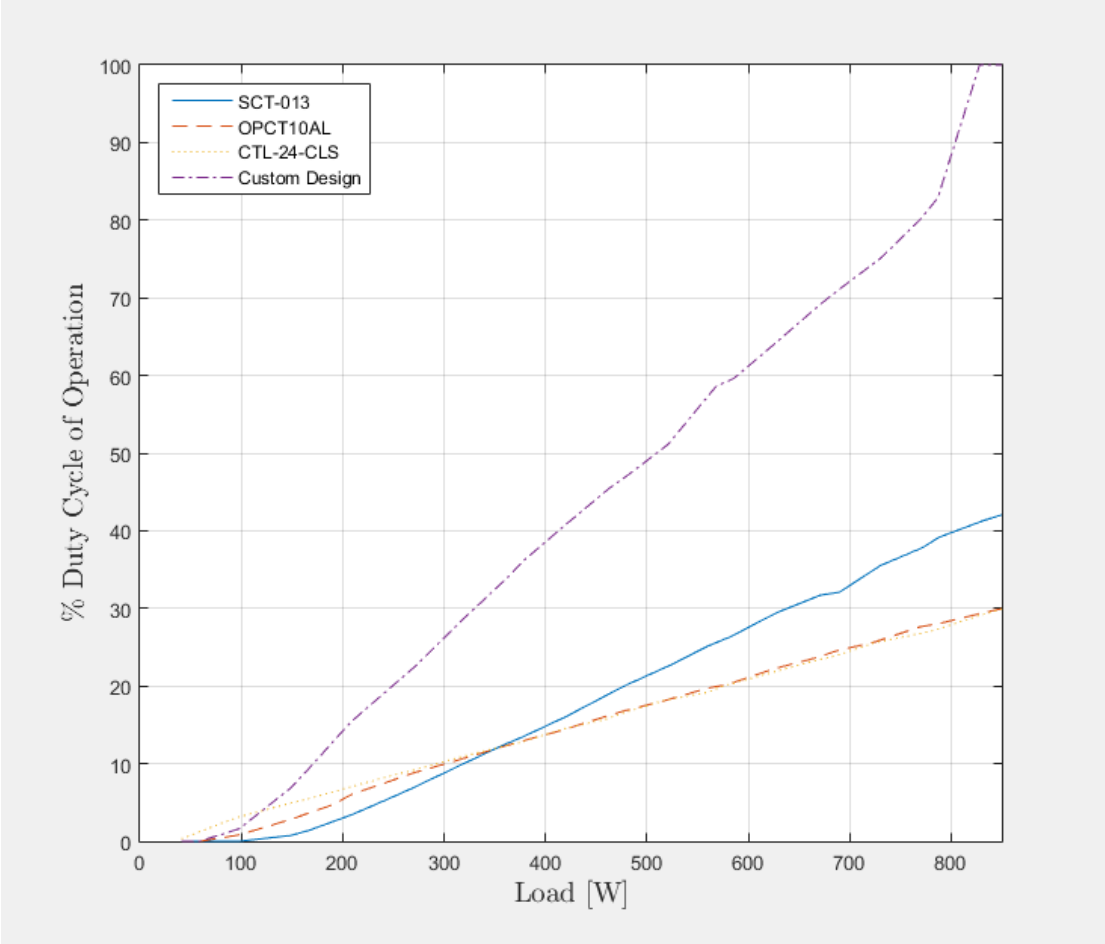

Figure 5.4: Chart showing performance of different tested CTs over a range of AC load power.

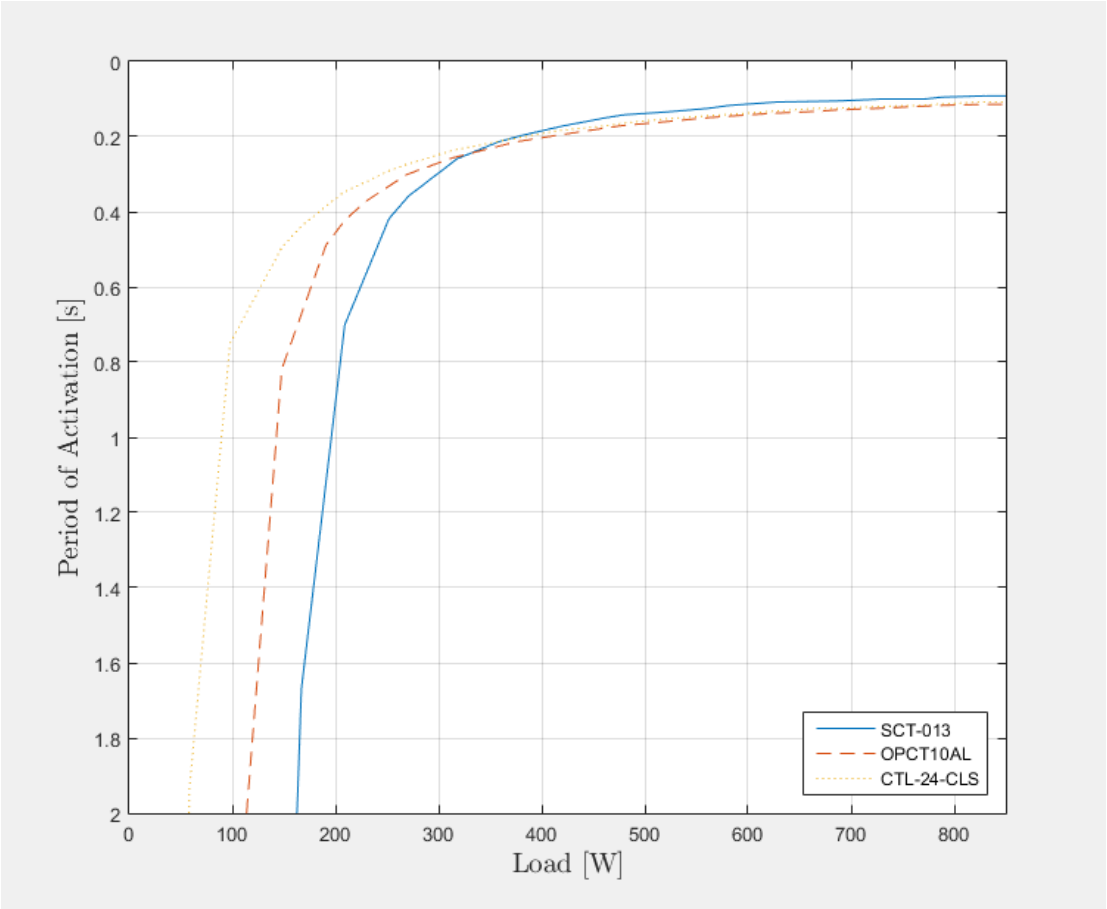

Figure 5.5: This chart demonstrates how the various tested CTs performed with small primary loads.

What could be seen is that the CT with a smaller core performed better at high primary loads, yet the larger core performed better with light loads. As can be seen in Figure 5.5 the larger ferrite core CT could activate the energy harvester at a lower minimum primary load. The medium sized core with its increased copper windings had more resistance on the secondary and because of this, it was unable to perform much better than the slightly larger ferrite CT at high loads.

For the input capacitance test, the CTL-24-CLS was set up with 220 and $440\mu F$ tantalum capacitors respectively. The results of these tests could be seen in Figure 5.6. As would be expected, doubling the input storage capacitance to the

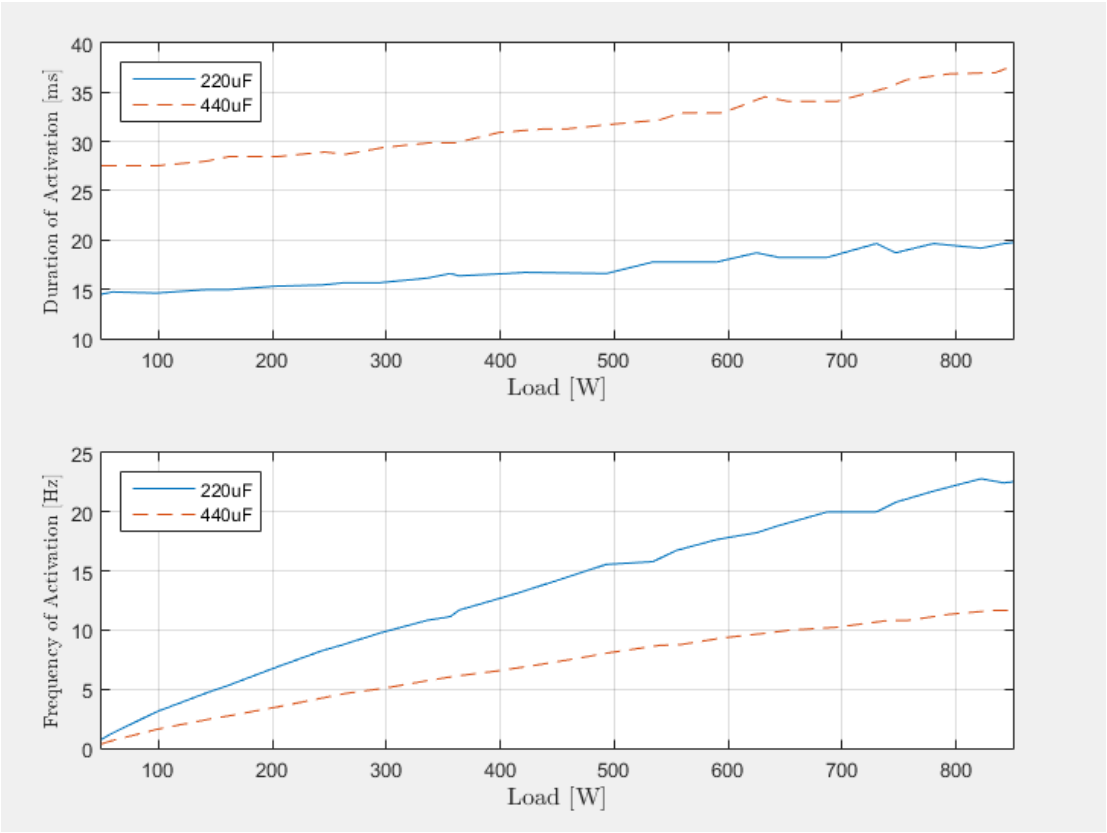

Figure 5.6: Data showing the effect of varying input capacitance on duration of buck converter activation (top) and frequency of activation (bottom).

energy harvester roughly doubled the time it took to charge the capacitor up which lead to the time between activations of the harvester also doubling. The tradeoff was that because there was twice the energy stored in the larger capacitance, the time that the harvester was active roughly doubled. The increase in performance tapered off at higher loads as the internal losses of the capacitors began to show a signigficant effect. This result showed that input capacitance must be carefully considered for each application as it was a balance between reasonably frequent sampling of the sensors to be applied, and adequate duration of supply voltage to perform a sensor measurement and data transmission.

For the next test the output capcitance was varied and the effects were recorded.

The input capacitance was set at $220\mu F$, switching inductance was set at $10\mu H$, and operating voltage was set at $3.3v$. The output capacitance of the buck converter is largely responsible for minimizing output ripple but it can also store a small amount of energy to be used at the moment the buck converter deactivates on the LTC3588. Increasing the capacitance on the output, however, also required more current flow to charge to the output voltage level and could decrease performance if raised too high. The results of the output capacitor testing can be seen in Figure 5.7.

It can be seen from the data that while duty cycle of operation increased with increased output capcitance up to about $100\mu F$, it began to be a diminishing return. It appeared to benefit the system when small AC loads were present and the duty cycle was low. When the buck converter was active more often, it had less time to charge the larger capacitance, and it began to lower the possible runtime of the system. An output capacitance of around $30 - 50\mu F$ appeared to offer the best all around performance for the tested load range.

Now that optimal capacitance values for the system have been observed, possible capacitor types were compared for their performance traits. The electrolytic, tantalum, and ceramic capacitor listed in Table 4.1 were those used in this experiment. The CTL-24-CLS again was used and the switching inductor was set at $10\mu H$ and the output at $3.3v$. Capacitance on the input was $220\mu F$ and $10\mu F$ on the output. The data in Figure 5.8 was normalized to $220\mu F$ as there were small variances in actual tested capacitance between compositions. The data showed that with ceramic capacitors, the duty cycle of activation of the system was increased about 40% compared to tantalum and electrolytic type capacitors. However they activated the LTC3588 for a shorter duration than the other types due to their quicker charge time. This issue can lead to more capacitance being

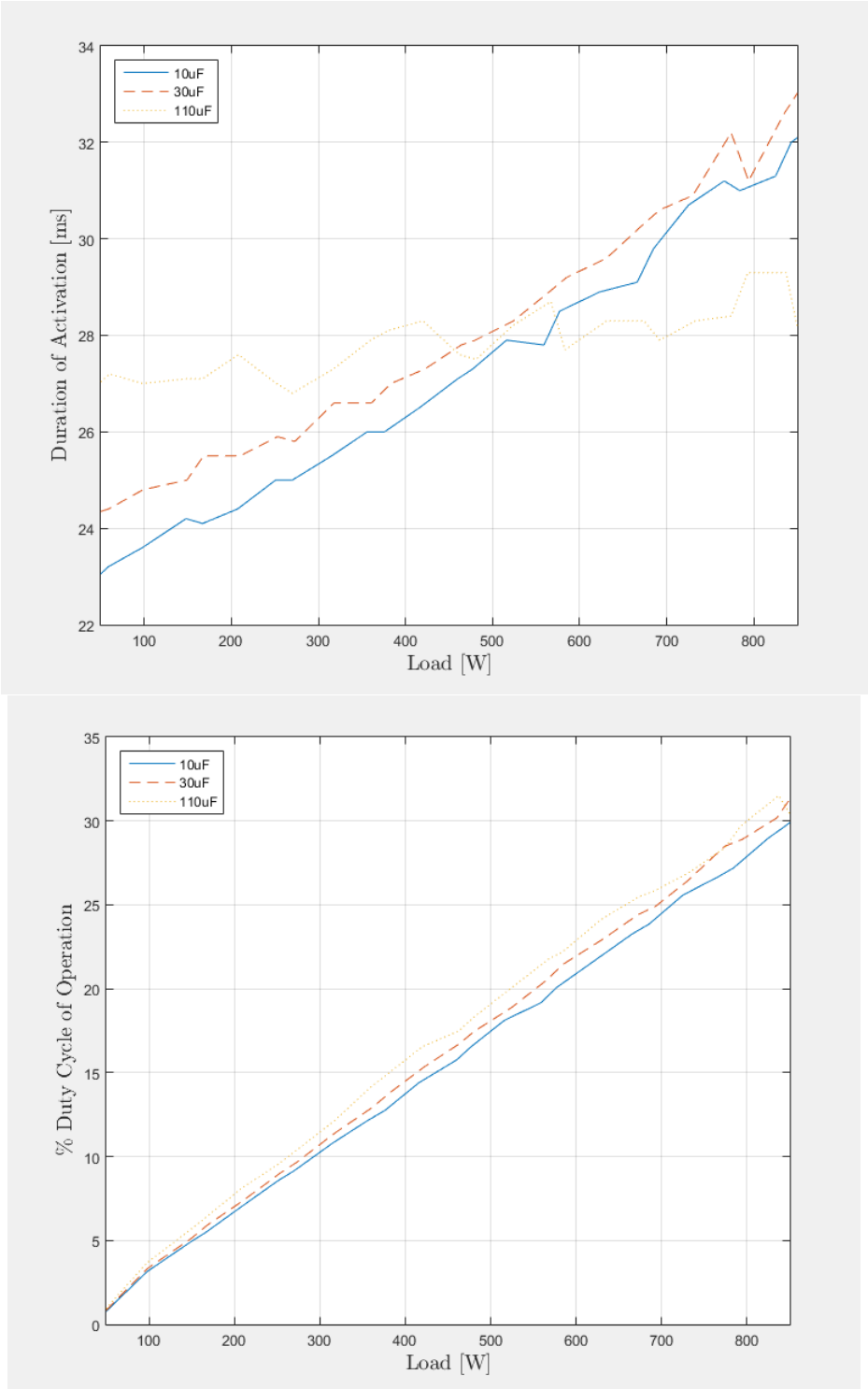

Figure 5.7: Data showing the effect of varying output capacitance on duration of buck converter activation (top) and overall duty cycle of activation (bottom).

required to match the same activation of the tantalum and electrolytic setups. Tantalum capacitors offer good performance for the price yet ceramic capacitors offer the lowest leakage and greatest performance when cost is not a design issue.

The last passive component variable for the buck converter was the switching inductor. As discussed in the previous section, increasing the inductance value beyond the recommended $10-22\mu H$ used in the example circuit from the datasheet could yield efficiency improvements, especially when AC voltages near the $20v$ shunted limit are present on the input. In this test tantalum capacitors were used and the same output voltage and capacitance value from the previous test were used. The tested inductors were $10\mu H$, $47\mu H$, and $220\mu H$ in value and the results can be viewed in Figure 5.9.

The data shows that while increasing the inductance does lead to some performance gains, the increase is modest approaching 5% when comparing $10\mu H$ to $220\mu H$. The increase in performance does not scale linearly and results in negligable performance gains above around $50\mu H$.

Finally, jumpers on the LTC3588 breakout board were modified so the output voltage could be set to $3.3v$, $2.5v$, and $1.8v$. Because the BLE radios to be considered for the design could operate off as low at $1.7v$, there were potentially large gains in system performance that can be achieved by operating the harvester at a lower output voltage. Testing with a single CT and a $220\mu F$ tantalum input capacitance, the data showed that because the input capacitance could be charged to a lower voltage in a shorter duration, there was a higher overall duty cycle of stable output voltage. This can be seen in Figure 5.10. Another interesting observation was that as the duty cycle of activation on the $1.8v$ test increased beyond 50%, the period of activation began to decrease as the on-time of the system exceeded the off-time. If the system were designed to send packets on

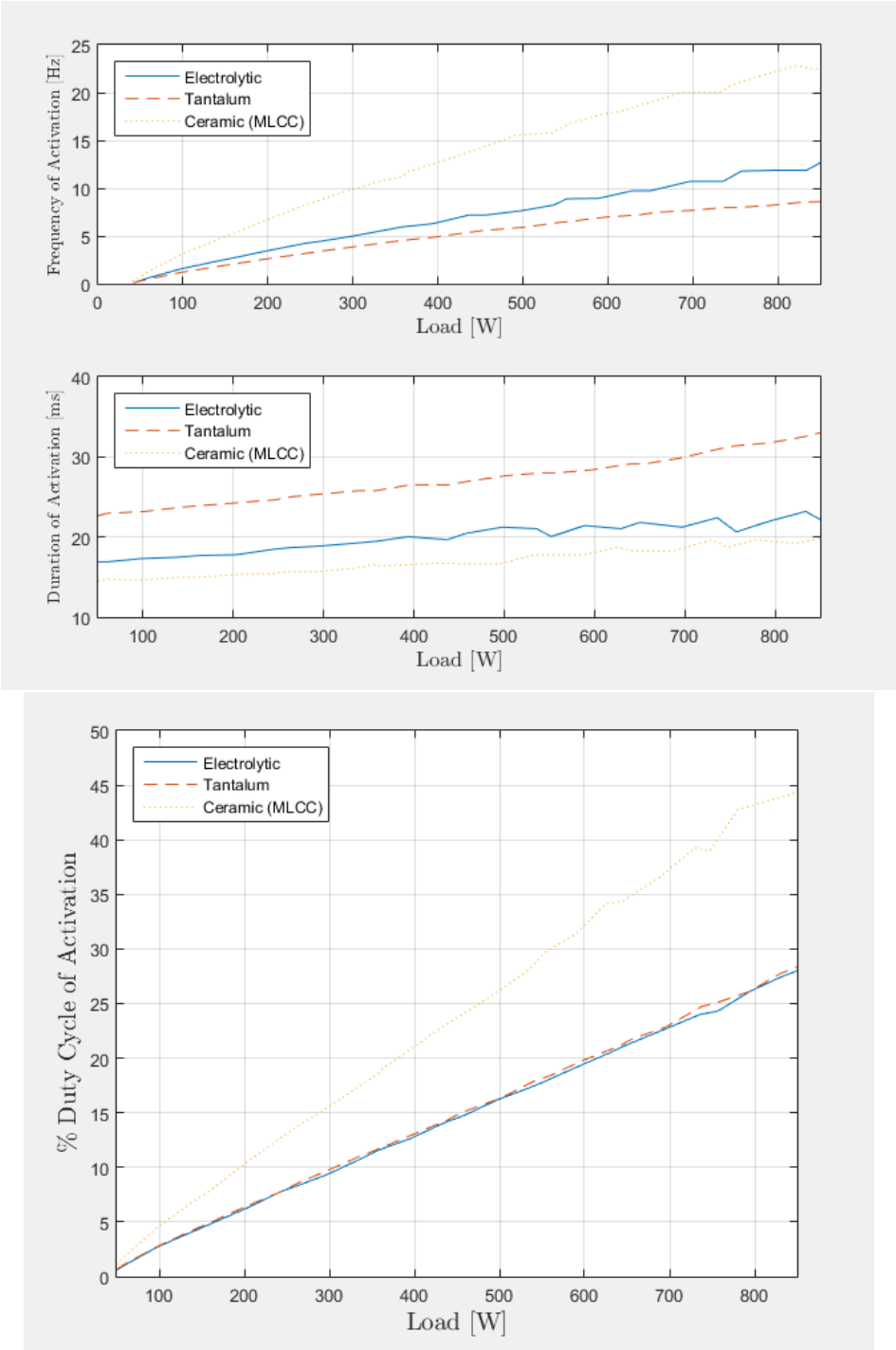

Figure 5.8: Data showing the effects of different capacitor types on frequency and duration of buck converter activation (top) and the overall duty cycle of activation (bottom).

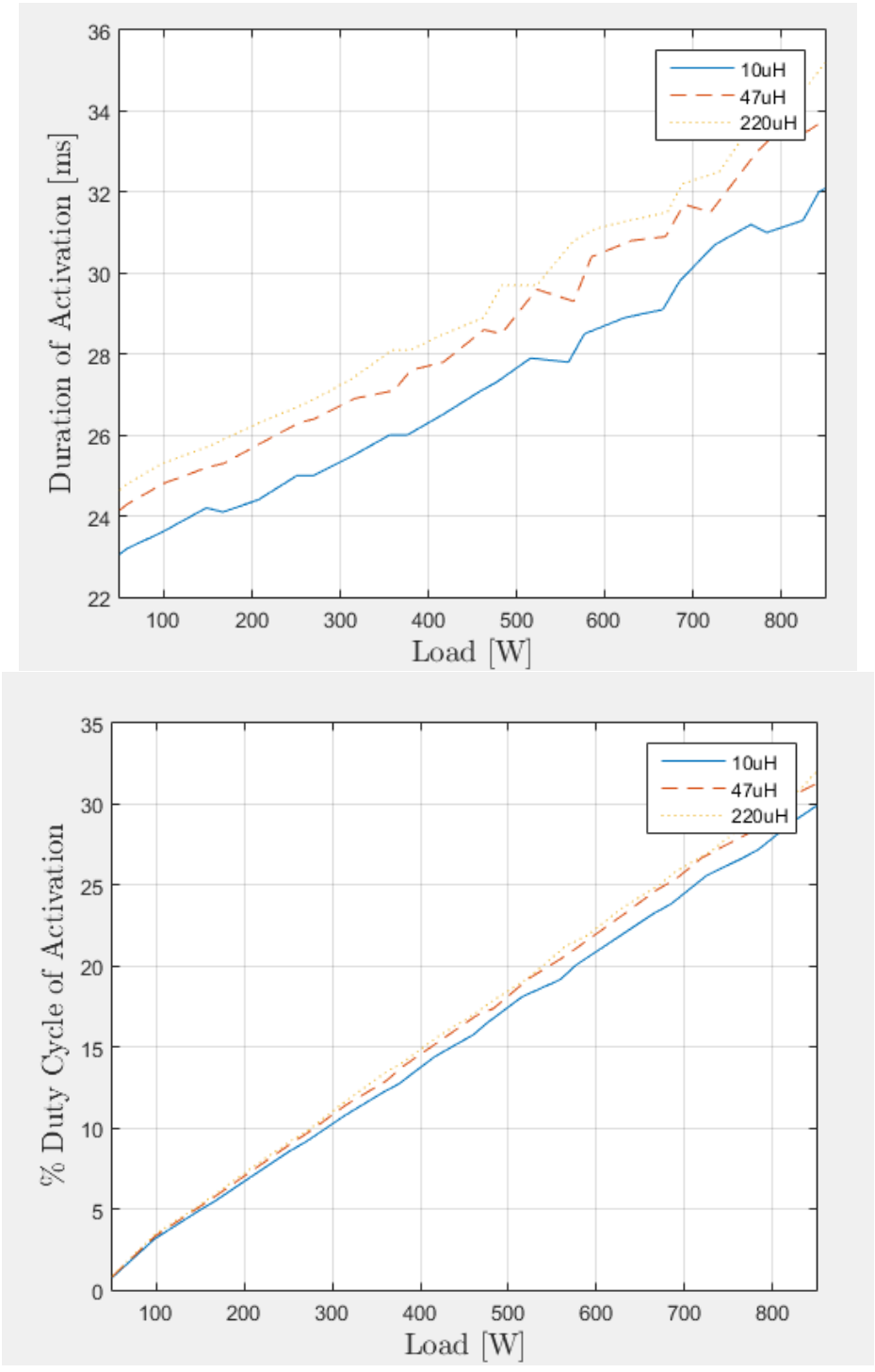

Figure 5.9: Data showing the effects of increasing switching inductance on frequency and duration of buck converter activation (top) and the overall duty cycle of activation (bottom).

activation it may be advantageous to limit the operation of the transceiver to a smaller window and continue to store the excess energy on the input capacitors for later use. A larger switchable input capacitance could be implemented for this scenario, storing energy while the system operates. The tradeoff to lowering the voltage output was that the amount of power available to the transceiver was then reduced. This power reduction could possibly restrict the range of wireless transmissions.

5.2.2 Power Consumption

In order to measure the power consumed from the AC line by the energy harvester, an ammeter in conjunction with an oscilloscope were used to examine the AC waveform entering the LTC3588 from the secondary winding of the CT. In this experiment, the custom laminated core transformer was used and the LTC3588 was operated in $3.3v$ mode with a $220\mu F$ input capacitance. With an AC line load of $800W$, the regulator is able to operate continuously. What is observed is a roughly square looking AC voltage that is about 20 volts peak-to-peak. This can be seen in Figure 5.11. This is a result of the protection diode in the LTC3588. The ammeter measures $22\mu A$ of current entering the regulator. Because the output is a roughly square wave, the RMS voltage is equal to the peak value of $10v$. The power consumed then can be roughly estimated at around $220\mu W$.

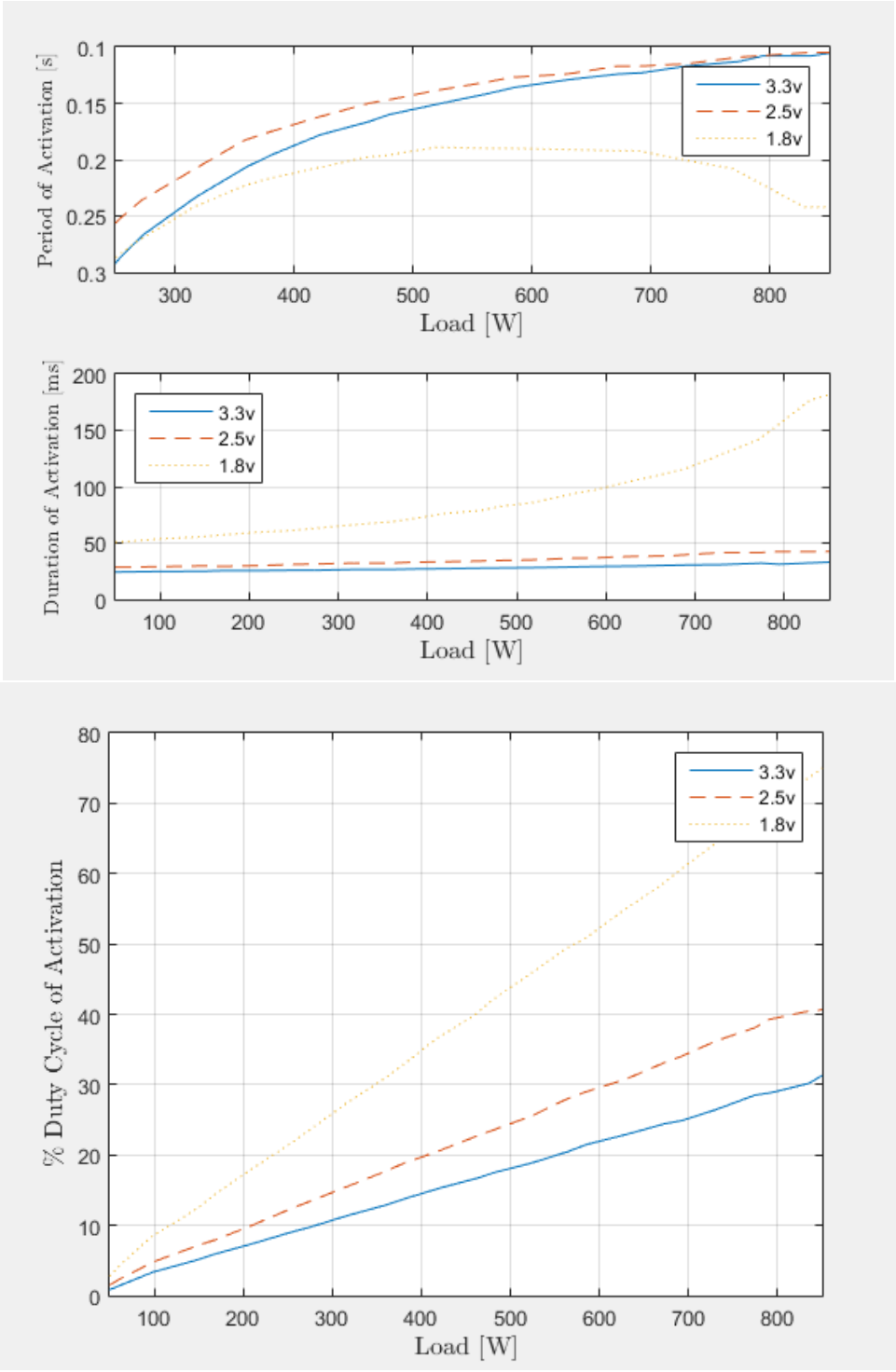

Figure 5.10: Effect of adjusting set output voltage of the LTC3588 on its period and duration of activation (top), and overall duty cycle of stable output voltage (bottom).

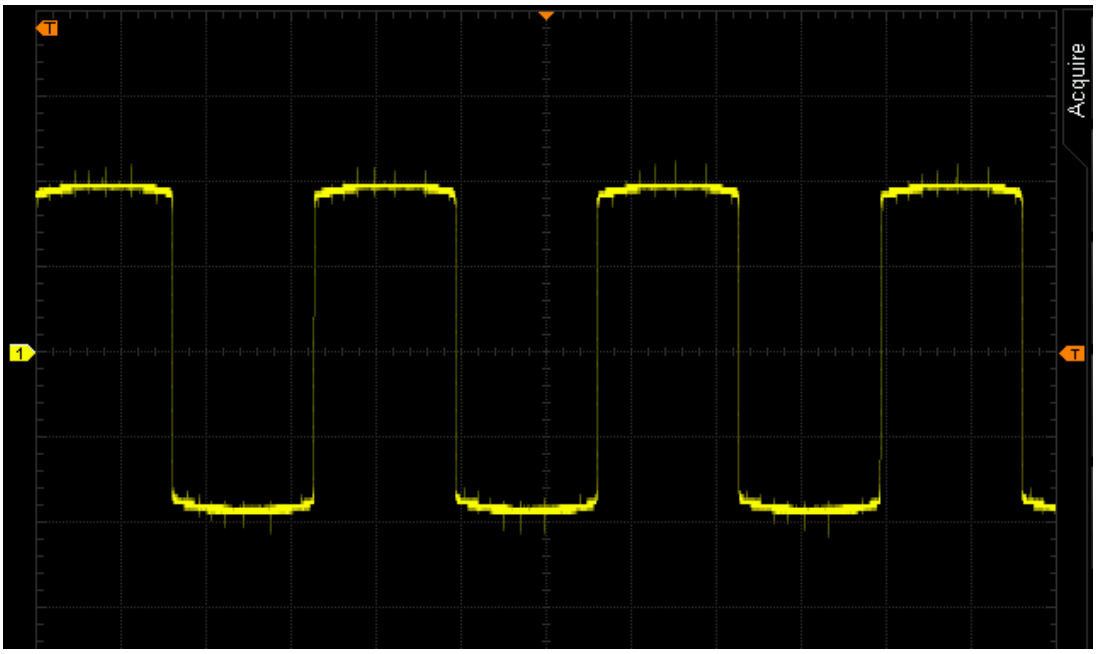

Figure 5.11: Oscilloscope capture of the AC voltage on the secondary winding of the current transformer. Vertical is set to 5v/div and horizontal is 5ms/div.

Chapter 6

Future Work

In this section, possible improvements for future designs of the energy harvesting current sensor are proposed. This section also serves to discuss ways the energy harvesting scheme can be employed for other sorts of data collection in remote locations.

6.1 Hardware Improvements

In the experiments performed, it has been proven that a laminated steel core is capable of transfering more magnetic energy than a ferrite core, and performs better for energy harvesting. However this comparison does not consider other core materials such as mu-metal, permalloy, or sendust which may offer greater performance with even greater permeability than the tested silicon steel. An investigation into the cost effectiveness of these exotic materials for thier possible performance gains could yield useful information.

6.2 Software Improvements

In order to make experimentation more simple, the tested SoC was run with a bootloader. The code also contained I/O and Bluetooth helper functions which contained some uneeded overhead. With more direct port manipulation and efficient programming methods, it is possible that a sampling rate higher than the $12kHz$ measured could be acheived. The SoC may also consume less power performing the necessary operations, thereby enabling the device to run continuously off a smaller AC line load.

With the added implementation of a hub device which collects data instead of the smartphone, the line voltage can measured in real-time as well. By measuring this the integral of voltage and current can be computed to get the actual power consumption. In its current form without voltage measurement, only current may be measured which in itself has uses such as the detection of overloads.

6.3 Alternate Applications

With the ability to use the ADC of an SoC to measure and transmit the voltage level of a current transformer output proven in experimentation, there is also the potential to implement sensors other than current transformers. In remote areas where access to an AC line is possible but conventional outlets are not, this energy harvesting scheme presented in this thesis may be used. Other sensors measuring air quality, temperature, humidity, pressure, etc. could be sampled by the SoC at a similar sampling rate as was measured in the experiments conducted, depending on the impedance of the sensors to be used.

Chapter 7

Conclusion

The proposed and tested system shows improvement in performance with a nearly linear relation to $120v$ AC line power in the tested $50 - 850W$ range. This means the frequency of useful data becomes greater at times of higher power usage, a quite advantageous trait of the system. This system combines the research fields of low power rectification and regulation and low-energy SoC tranceivers. The research done adresses each facet of the energy harvesting system design. Results show that with specialized current transformers, performance can be increased beyond previous related harvesting designs, approaching continous operation for loads above $750W$ or $6.25A$. Careful tuning of the circuit components can result in operating performance tailored to the load range expected and throughput desired. This research represents a first step into the investigation and ultimate fabrication of a complete energy harvesting system.

Bibliography

[1] B. Campbell and P. Dutta. Gemini: A non-invasive, energy-harvesting true power meter. Technical report, University of Michigan, 2014. University of Michigan. https://web.eecs.umich.edu/ prabal/pubs/papers/campbell14gemini.pdf.

[2] S. DeBruin, B. Campbell, and P. Dutta. Monjolo: An energy-harvesting energy meter architecture. Technical report, University of Michigan, 2013.

[3] R. Faltus, M. Jánê, and T. Zedníĉek. Storage capacitor properties and thier effect on energy harvester performance.

[4] David J. Griffiths. *Introduction to Electrodynamics (3rd ed.)*. Prentice Hall, 1998.

[5] T. Itoh. Ultra low power wireless sensor nodes for expanding application of the internet of things, 2016.

[6] V. Lee. Energy harvesting for wireless sensor networks. Technical report, University of California at Berkeley, 2012. https://www2.eecs.berkeley.edu/Pubs/TechRpts/2012/EECS-2012-141.pdf.

[7] Linear Technology. *LTC3588 Datasheet*. http://cds.linear.com/docs/en/datasheet/35881fa.pdf.

[8] J. Mayernik. Department of energy (doe) buildings energy data book. Technical report, Department of Energy, 2011. https://openei.org/doe-opendata/dataset/buildings-energy-data-book.

[9] Nordic Semiconductor. *nRF51822 Datasheet*. https://www.nordicsemi.com/eng/Products/Bluetooth-low-energy/nRF51822.

[10] Nordic Semiconductor. *nRF52832 Product Specification v1.4*. http://infocenter.nordicsemi.com/pdf/nRF52832_PS_v1.4.pdf.

[11] NXP. *QN908x Ultra low power Bluetooth 5 system-on-chip solution*. https://www.nxp.com/docs/en/nxp/data-sheets/QN908x.pdf.

[12] P3 International. *Kill-A-Watt*. http://www.p3international.com/products/p4400.html.

[13] ST. *BlueNRG-2 Datasheet*. http://www.st.com/en/wireless-connectivity/bluenrg-2.html.

[14] Texas Instruments. *CC2650 SimpleLink™ Multistandard Wireless MCU*. http://www.ti.com/lit/ds/symlink/cc2650.pdf.

[15] U.S. Environmental Protection Agency. *ENERGY STAR® Program Requirements for Single Voltage External Ac-Dc and Ac-Ac Power Supplies*. https://www.energystar.gov/ia/partners/product_specs/program_reqs/eps_prog_req.pdf.

[16] Q. Xu, I. Paprotny, M. Seidel, R. White, and P. Wright. Stick-on piezoelectronic ac current monitoring of circuit breaker panels. 2013.